Electronics and Electrical Engineering

AIMS Electronics and Electrical Engineering, 3(4): 370–381.
DOI: 10.3934/ElectrEng.2019.4.370
Received: 12 August 2019
Accepted: 06 November 2019
Published: 15 November 2019

http://www.aimspress.com/journal/ElectrEng

Research article

In-junction-plane beam divergence stabilization by lateral periodic structure in wide-stripe laser diodes

Andrzej Maląg[1], Grzegorz Sobczak[2,*], Elżbieta Dąbrowska[1] and Marian Teodorczyk[1]

[1] Łukasiewicz Research Network – Institute of Electronic Materials Technology, 133 Wólczyńska str., 01-919 Warszawa, Poland
[2] Łukasiewicz Research Network – Institute of Electron Technology, 32/46 Lotników av., 02-668 Warszawa, Poland

* **Correspondence:** Email: grzegorz_sob@o2.pl.

Abstract: This paper describes the way to stabilize in-junction-plane optical field distribution and emitted beam divergence in high-power 970-nm-band laser diodes (LDs). This is done by introducing a lateral periodic structure into the LD's wide-stripe-waveguide, designed to prefer and stabilize the selected (resonant) high-order lateral mode. According to modeling, in CW operation the gain equalization of lateral modes due to thermal index guiding leads to beam divergence stabilization by incorporating the modes up to the resonant one and cutting out higher ones. This was demonstrated experimentally in a wide drive current range. Such stability of a non-Gaussian laser beam profile with steep slopes can be interesting for many applications. Thanks to the drive current flow control by the periodic structure, the effects typical for conventional wide-stripe LDs, such as lateral current crowding, carrier accumulation at stripe edges and optical far-field blooming are not observed.

Keywords: laser diodes; waveguiding in junction plane; in-plane directional characteristics; beam divergence stabilization

1. Introduction

Thanks to high electrical-to-optical power conversion efficiency, small sizes, as well as suitability for various forms of integration at wavelengths precisely determined in a technological process, laser

diodes (LDs) are one of the key elements in optoelectronics. Despite the known advantages and the wide range of applications, some areas are not available for LD use, however, due to poor quality of the emitted beam. In wide-stripe (WS) gain-guided constructions typical for high-power LDs, lateral (in the junction plane) distributions of the optical field in the cavity and then the emitted beam are unstable in time and as a function of a drive current. This instability of the combination of a WS-multimode structure and filamentation (originated from micro-nonuniformities of an active region) is a result of several dynamically interacting, nonlinear effects, such as gain saturation, thermal index guiding and free-carrier index antiguiding. In continuous operation (CW) strengthened thermal index guiding causes additional field destabilization, which is seen as uncontrollable variations of the emitted beam distribution in the far-field with the drive current changes.

Improvement of the beam quality in the junction plane has been of interest for a long time – there are numerous theoretical and experimental investigations aimed at explaining the mechanisms and mastering the problem [1–10]. The concepts of WS waveguide modification leading to 'ordering' light-wave propagation, which in turn would improve beam stability, can be shortly summarized as follows. First, the 'natural' idea to suppress filamentation by replacing the wide-stripe with a series of narrow nearby active stripes led to the phase-locked array (PLA) design [11–16], sometimes termed as photonic crystals [17]. Another concept is to ensure a lateral optical field distribution in the wide stripe stable enough to overcome the above-mentioned fluctuations. Various constructions have been proposed for this purpose, including MOPA and flared-waveguide LDs [18], spatial filtering by stripe edge modifications [19,20], 'profiling' the lateral gain and optical field distribution via a multi-stripe tailored p-contact design [21], and lateral thermal lensing reduction via 'pedestal' LD mounting (with a risk of some device's thermal resistance increase) [22,23]. Another possibility described in the literature is external beam stabilization by optical feedback or optical injection [6,24]. Predominantly, the design modifications in the junction plane are aimed at enhancement and stabilization of the fundamental lateral mode by suppression of higher-order ones [18–23,25–32]. This is difficult when a wide laser drive current range is desirable and symptoms of beam instability still remain. A recent proposal consists in emitted beam stabilization by superposition of low- and high-order lateral modes constrained by a lateral periodicity superimposed on a wide-stripe waveguide [33]. Then, a two-dimensional periodic 'Spatial-Current-Modulated' (SCM) structure was described [34], where mutual (lateral and longitudinal) periodicity perturbations are shown to lead to beam stabilization in the wide LD's drive current range, with prevailing content of low-order modes. The mechanism of far-field (FF) and near-field (NF) distributions stabilization over the drive-current range seems not to be explained clearly enough, however.

This paper refers to the earlier presented concept of lateral periodic structure (LPS) built into an LD's WS waveguide by spatially selective techniques (ion implantation [33], chemical etching) in order to stabilize optical field distribution in the junction plane. Periodic current flow and gain profiles (as sketched in Figure 1; continuous in the longitudinal direction) prefer and stabilize high-order WS-lateral-eigen-modes of spatial distribution close to LPS, in relation to the fundamental and low-order ones (this differentiates LPS-LDs from geometrically similar PLAs where electrically separated narrow single–mode stripes are optically coupled to each other). Such stabilization over a wide range of LD's drive current and optical power in pulsed and CW operation by the LPS built into asymmetric InGaAs/AlGaAs/GaAs heterostructure by chemical etching is described here. The resulting lateral beam divergence stabilization over the LD's CW operating range is evidenced.

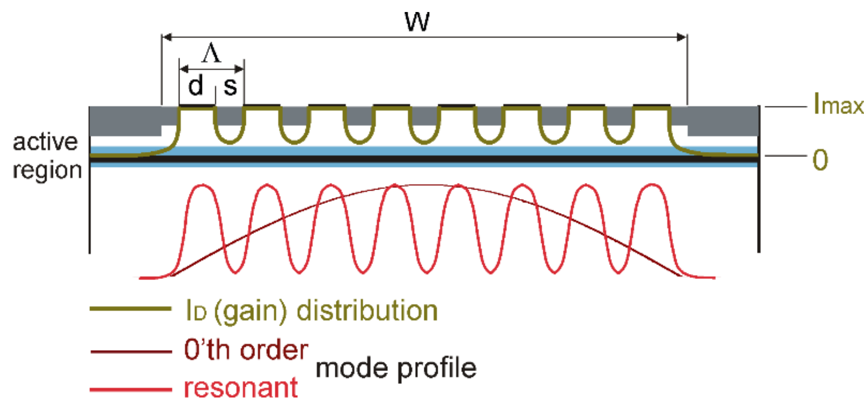

Figure 1. A schematic cross-section (mirror-plane) of LPS-LD. Insulating (etched-away) areas are marked in gray. The high-gain and the isolating stripe widths *d* and *s*, respectively, as well as the period Λ are indicated. The barrier layers surrounding quantum well (QW) are denoted as 'active region'. The lateral current spreading/gain distribution (dark yellow line) and optical field intensity profiles (red lines) are shown schematically.

In the following, the design and technological issues, then mode-gain simulations in LPS-LDs and in conventional 'reference' wide-stripe devices (WS-LDs) under pulsed and CW conditions are discussed in Section 2. Then, in Section 3, in connection with the simulation results, the experimental short-pulse and CW near-field (NF) and far-field (FF) emission characteristics of high-power LPS- and WS-LDs are comparatively analyzed, indicating the stabilization effect of the LPS. Section 4 presents the conclusions.

2. Materials and LPS design – lateral mode selection

The scheme in the plane perpendicular to the waveguiding direction (i.e. in the LD's mirror plane) of the LPS built into the asymmetric heterostructure is shown in Figure 2 together with the corresponding vertical (perpendicular to the junction plane) heterostructure refractive index profile and the calculated optical field intensity distribution of the fundamental transverse mode. The SEM photograph (Figure 3) shows such asymmetric InGaAs/AlGaAs/GaAs heterostructure designed for 970 nm (analogous to the earlier one designed for 810 nm [35]), with the LPS built in by selective wet-etching. It consists of a series of electrically conducting active stripes (of width *d*, numbered 1, 2…..N) interlaced with insulating trenches (of width *s*, Schottky isolation), both no wider than the native filament size (~6 µm [36]). The LPS period $\Lambda = d + s$. Thanks to weak optical field penetration into thin *p*-cladding layer (with no risk of absorption in the contact layer and metallization, as seen in the right part of Figure 2), a relatively shallow LPS is sufficient for current flow control and gain shaping in the active region. Due to lateral current spreading under the isolating stripes (*s*), current density minima are formed beneath their centers (as sketched in Figure 1) and the resulting lateral electronic gain modulation profile at the active layer depends on the *p*-cladding resistivity and on the LPS *d/s* ratio and etching depth. To estimate the impact of this electronic gain profile on the mode-gains of lateral eigen-modes of the LD's WS waveguide (using the Photon Design's FIMMWAWE software), the isolating trench regions (*s*) have been modeled as sets of five constituent vertical slices of various gain in the active layer, as illustrated in Figure 2.

Arbitrarily introduced sets of electronic gain values in slices (with respect to assumed uniform electronic gain in the active stripes (*d*) [37]) serve to model various constructions, including both electrical and geometrical properties of *p*-cladding's LPS.

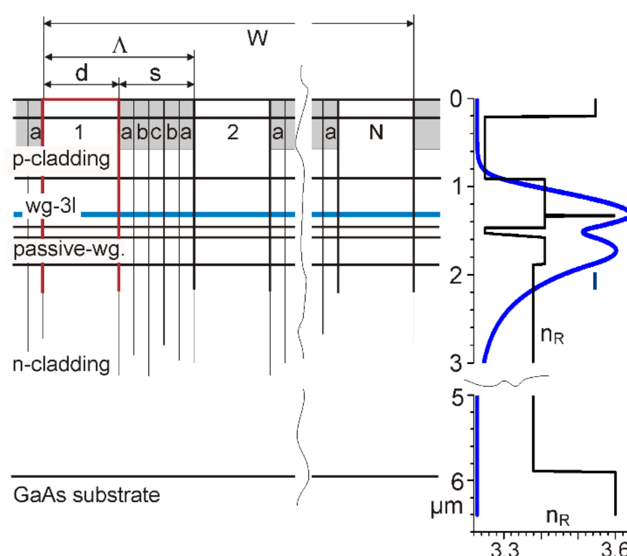

Figure 2. LPS scheme for numerical modelling. The gain relation (in the active layer) $g_c < g_b < g_a$ of respective vertical slices *c, b, a* within unpumped stripes (*s*) and gain $g_a <$ gain in the active stripes (1, 2, ….N, of the width *d*) is a rule maintained for all calculated versions. Various sets of g_x-values (*x: c, b, a*) can model various LPS constructions. The gray areas in the picture show fragments of the heterostructure removed by etching. At the right side: the refractive index profile (n_R) and calculated optical field intensity distribution (*I*) of the fundamental transverse mode in the InGaAs/$Al_xGa_{1-x}As$/GaAs heterostructure waveguide. Abbreviations: *wg3l* – waveguiding triple-layer including QW (blue line), *pass-wg*. – passive waveguide.

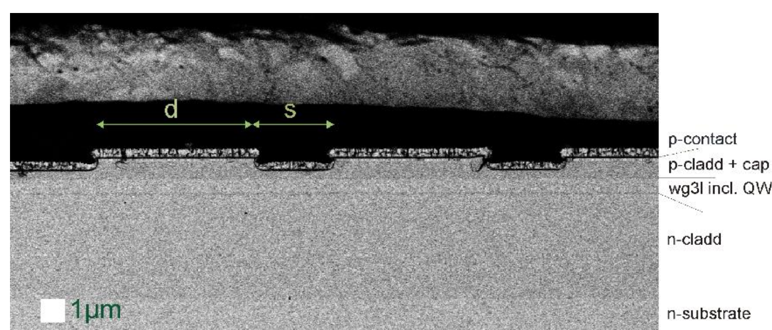

Figure 3. SEM photograph (ESB – energy selective backscattering mode) of a fragment of LPS built into the InGaAs/AlGaAs/GaAs heterostructure by wet chemical etching (cross-section parallel to the mirror plane). Heterostructure layers (or groups of layers) are marked in agreement with Figure 2: *p*-contact CrPt, Au-electroplated; *cap* GaAs, $p \geq 2E19$ cm^{-3}; *p-cladding* $Al_{0.5}Ga_{0.5}As$, p = 5E17 cm^{-3}; *wg3l* $Al_{0.2}Ga_{0.8}As$+InGaAs QW, undoped; *pass-wg*. $Al_{0.2}Ga_{0.8}As$, n = 5E16 cm^{-3}; *n-cladding* $Al_{0.25}Ga_{0.75}As$, n = 1E17 – 2E18 cm^{-3} (graded). The pumped stripes of width d = 6 μm, Schottky-isolated gaps (s = 3 μm) and etching depth can be seen. $\Lambda = d + s = 9$ μm.

In a ‘reference’ gain-guided WS-LD structure of stripe width W (close to (N $\times \Lambda$) of the LPS) and of a given electronic gain in the active region, the fundamental lateral mode (n = 0) has the highest gain, and then the calculated higher-order mode-gains gradually fall due to worsening overlap (Figure 4, plot 1). With the LD’s drive current (I_D) increase above the 0’th-mode threshold, enabling higher-order modes into laser operation widens the lateral FF distribution of the emitted beam (no above-threshold gain saturation in WS-LDs is assumed in the model). This ‘intrinsic’ FF widening is not connected with carrier-transport-related effects, such as lateral current crowding or carrier accumulation at stripe edges [7–10,23,28]).

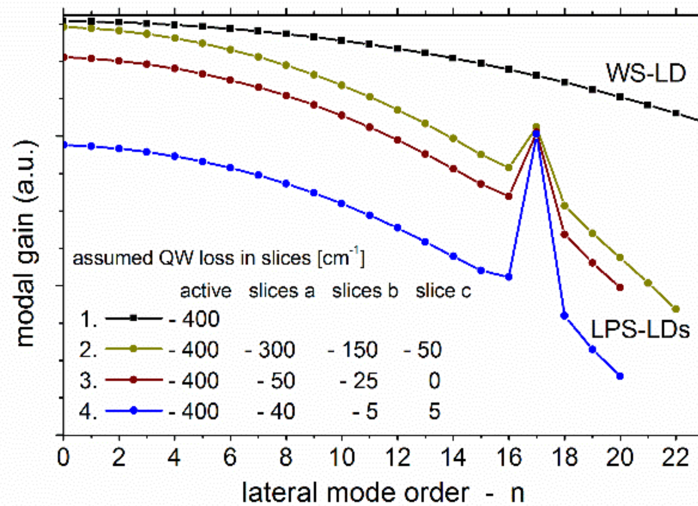

Figure 4. Calculated mode-gain distributions for pulse-operated WS-LDs (plot 1) and LPS (N = 18) LDs – plots 2 - 4 for exemplary, increasing LPS modulation depths. Assumed loss/gain values in sequent slices a, b, c (in QW layer) are shown in the legend.

In the case of LPS insertion into WS low-mesa, the fundamental and the lowest-order eigen-modes of WS waveguide still propagate as in a uniform medium of a gain averaged over the period (Λ). Calculated gains of higher-order modes quickly decrease, however, due to worsening spatial matching with the LPS gain distribution. Only for the ‘resonant’ n = N – 1 mode (and eventually for the nearest neighbors) the gain sharply increases due to spatial fitting (the best overlap). The gain ratio of the fundamental and the resonant modes $R_{gmod} = g_{0mod}/g_{rez\ gmod}$ depends on the LPS gain/loss profile and on the d/s ratio. This is shown in Figure 4 for exemplary gain modulation profiles (plots 2 - 4), for established through this work d/s = 6/3 [µm/µm] and N = 18. The selected parameters d and s result from earlier trials [37], they are below the native filament size and can be formed by conventional photolithography. The cumulative contact stripe width 108 µm is close to that of conventional WS LDs. For $R_{gmod} > 1$ (plots 2 - 3 in Figure 4) the lasing is expected to start with the dominant lowest-order modes, while the resonant and nearest modes can be enhanced at higher I_D, depending on the R_{gmod} value. For $R_{gmod} < 1$, in turn (plot 4), the predominance of the resonant mode at LPS-LD’s threshold, and then gradual switching-on of low-order modes with increasing I_D is expected. These gain profile variations influence the calculated average gain level when the assumed electronic gain in active stripes is kept constant (e.g. 400 cm^{-1} in Figure 4).

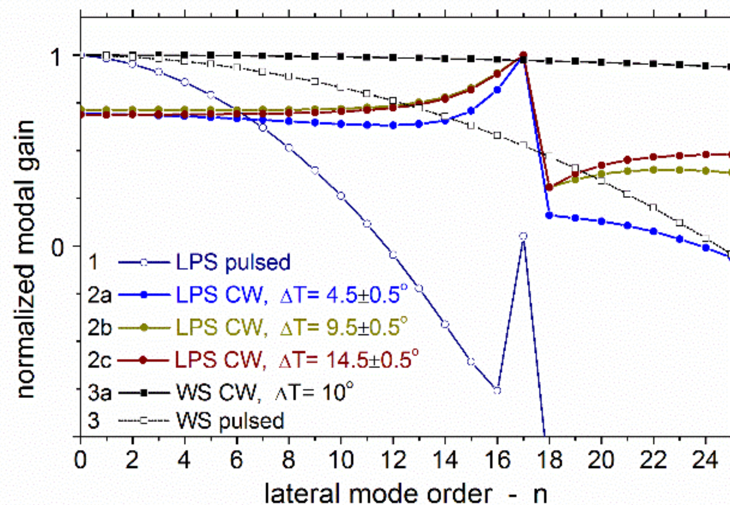

Figure 5. Calculated gain distributions (normalized to their maxima) of WS-LDs and LPS (N = 18) LDs under pulsed and CW conditions. The mode-gain equalization due to thermal index guiding in WS-LDs is seen in plot 3a when compared to plot 3 (equivalent to plot 1 of Figure 4). In LPS-LD, thermal index guiding causes preference of modes of the range $0 < n <$ N-1 (plots 2a - c) compared to the gain distribution in pulse-operation – plot 1 (the same as plot 3 in Figure 4). Plots 2a - 2c illustrate mode-gain equalization due to strengthening thermal index guiding for increasing active stripe temperature caused by increasing the drive current.

In the CW analysis, the inclusion of thermal index guiding in the active stripe [38,39] equalizes the calculated lateral mode gains, covering the mode-discriminating mechanism described above (by varying spatial overlap). For WS-LD it is shown in Figure 5-plot 3a for CW operation with an assumed temperature rise of the active layer ΔT = 10 K (then ΔT tends to 0 K at heterostructure surfaces in all modelled cases). This is compared with the gain distribution for short-pulse-operation – plot 3. The calculated equalization means that many lateral modes can be excited simultaneously, with a possibility of unrestricted competition. The lack of control over this effect gives rise to the optical field and emitted beam instabilities. In LPS-LDs, in turn, the mode-gain equalization effect includes lateral modes of the orders $0 < n <$ N-1, as seen in Figure 5-plots 2a - c, compared to plot 1 for pulse operation (this equalization with a slight gain rise of modes close to the resonance results in a change from $R_{gmod} > 1$ to $R_{gmod} < 1$). The gains of further modes ($n >$ N-1) are sharply reduced due to the spatial mismatch with LPS. This restricts and stabilizes the emitted beam divergence. The effect depends on the thermal index guiding magnitude, characterized here by the active region temperature rise ΔT (generally attributed to I_D variations, irrespective of device construction details). This is shown by plots 2a - c (Figure 5) for ΔT = 5 - 15 K, respectively, with temperature fluctuations between the active (d) and passive stripes (s) of 1 K (in the active layer), in agreement with earlier results [14,37,39]. According to these results, the resonant mode preference, especially with respect to modes $n >$ N-1, is slightly reduced with increasing ΔT, but still the gain difference restricts the emitted beam profile expansion in a wide I_D range, which points to the beam divergence stabilization ability of the LPS. At the same time, gain equalization allows for nearly uncontrolled competition of optical field components from the range $0 < n <$ N-1.

3. Experimental – pulse and CW characteristics of LPS LDs

LPS LD structures of the total width N × Λ = 18 × 9 = 162 µm (a fragment shown in Figure 3), wet-etched atop of previously etched mesa stripes of width *W* = 170 µm were made from the asymmetric 970-nm-emitting InGaAs/AlGaAs/GaAs heterostructure wafer. Etching of trenches (*s*) through the *p*+ contact layer leads to local Schottky isolations at the metal-AlGaAs interfaces. The 'reference' He+-implantation-isolated WS structures of *W* = 190 µm have been manufactured in parallel, from the same heterostructure. The etching depth and the He+-implantation range are similar. Exemplary P-I-V pulsed characteristics of unmounted LDs made from both groups (of common cavity length *L* = 3 mm and LR/HR facets coatings) are shown in Figure 6. Threshold currents and external efficiencies as well as series resistances are similar; the differences are within the range of technological dispersion over the wafer. This demonstrates that no extra optical loss or electrical hindrances were introduced by inserting the LPS into the heterostructure.

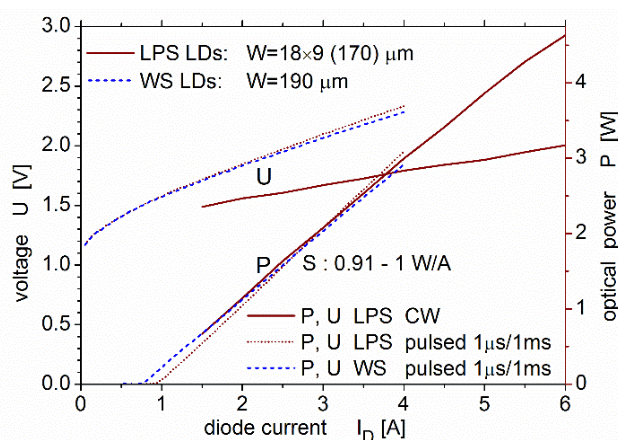

Figure 6. Comparative P-I-V characteristics of pulse-operated (1 µs and 1 ms pulse duration and repetition; unmounted) and of CW-driven LPS-LDs, as well as of pulse-operated 'reference' WS-LDs. All the diodes manufactured in most common technological process from the asymmetric InGaAs/AlGaAs/GaAs heterostructure. The observed difference in series resistances results from different conditions: test-probe measurements of unmounted chips and measurements of soldered and wire-bonded chips in pulsed and CW conditions, respectively.

A set of pulsed NF- as well as pulsed and CW FF-characteristics of an exemplary LPS-LD is shown in Figure 7. The relatively shallow intensity modulation depth seen in the NF characteristics (Figure 7a) indicates the dominance of lowest-order modes in this diode over the applied I_D range. This corresponds with plots 2 or 3 ($R_{gmod} > 1$) in Figure 4. In the pulsed FF characteristics (Figure 7b) this dominance is even more pronounced, but the lateral beam divergence is stabilized by high-order (close to resonant) modes. The share of these modes grows rather slowly with I_D increase, which can be an indication of a partial, above-threshold gain saturation effect due to an optical field 'ordering' by the periodicity. Divergence stabilization effected by the LPS makes it independent of *L*, as illustrated in Figure 8a-b, unlike in conventional gain-guided WS LDs.

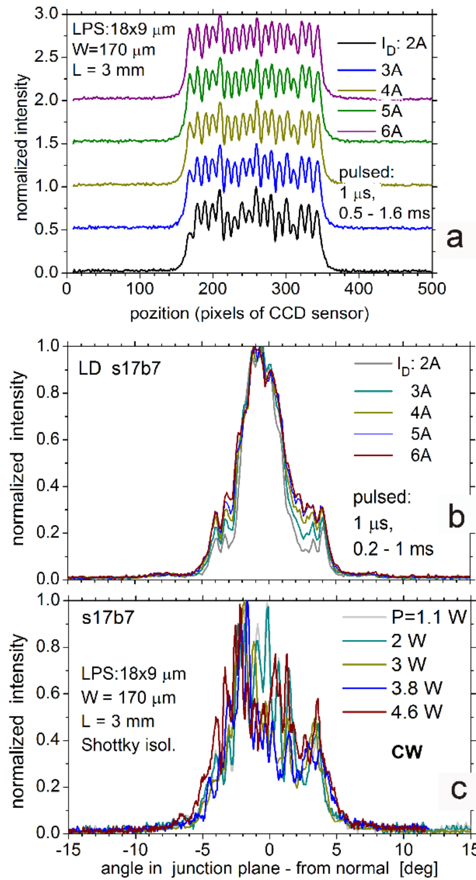

Figure 7. NF-pulse-characteristics (a), FF pulse characteristics (b) and FF CW characteristics (c) of LPS LD.

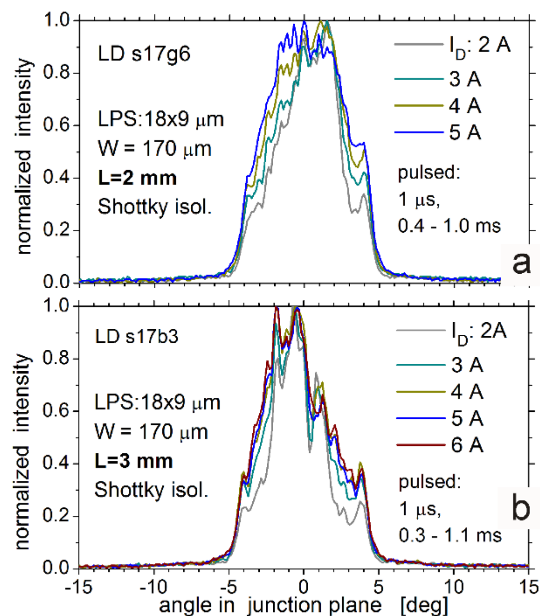

Figure 8. Pulsed FF characteristics of LPS-LDs with R_{gmod} > 1 of various L. Pulse duration: 1 μs, repetition varied to prevent CCD camera blinding.

Diodes prepared for CW operation were In-soldered on Cu heatsinks and wire-bonded. The representative CW P-I-V characteristics of the LPS-LD are shown in Figure 6 together with the pulse characteristics of unmounted devices. The CW characteristics start from I_D = 1.5 A, which is the low current limit of the CW source used (ILX Lightwave model LDX-36085-12).

The CW FF characteristics of the LPS-LD is shown in Figure 7c. The beam divergence stabilization over the applied I_D range results from the restricted $0 < n <$ N-1 range of 'included' modes, as explained in Figure 5 (plots 2a-c). Compared to the pulse characteristics (Figure 7b, the same diode before mounting), the increased share of high-order modes is caused by thermal index guiding and mode-gain equalization (plots 2a-c compared to plot 1 in Figure 5). At the same time, the competition of the included modes is seen as intensity fluctuations of their interference fringes with ID changes in CW FF patterns.

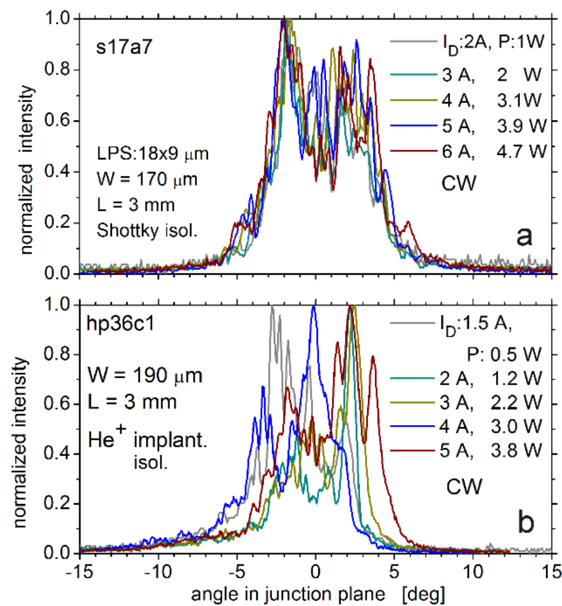

Figure 9. CW FF characteristics of the LPS LD (a) and, for comparison, CW FF characteristics of the WS LD made from the same heterostructure (b).

The CW FF characteristics of another LPS-LD and of a 'reference' WS-LD are shown in Figures 9a and 9b, respectively. Even though the lateral beam profiles can differ for individual LPS-LDs (as seen in Figures 7c and 9a) due to heterostructure micro-nonuniformities, the LPS stabilizes the beam divergence (i) of LDs from the same wafer (determined by W and N) and (ii) as a function of I_D. In comparison with the unstable FF patterns of WS-LD (Figure 9b) the progress in the lateral optical field distribution control is clear.

LDs with various LPS modulation depths resulting in different (stabilized) FF characteristics have been investigated as well [33,37,40]. Filamentation reduction has been demonstrated [33,37]. Moreover, such effects as lateral current crowding, carrier accumulation at stripe edges or the resulting thermal FF blooming that are common for CW-operated WS-LDs [7–10,23,28,41], have not been observed in LPS-LDs.

4. Conclusions

The lateral periodic structure (LPS) built into wide-stripe-LD design can stabilize its optical field distribution and the emitted beam divergence in the junction plane over a wide drive current

range. The stabilization is achieved by restricting the lasing lateral-mode-orders to range $0 < n <$ N-1 and cutting out higher ones (N is the number of stripes in the LPS). The lateral beam divergence is determined by LD's active stripe width (W) and N. In CW operation, thermal index guiding flattens the gain distribution of lasing modes, resulting in relative enhancement of mode-orders close to N, which is observed as an increase of optical power at the sides of the FF pattern.

Formation and control of a periodic current flow by LPS prevents such effects as lateral current crowding, carrier accumulation at stripe edges and the resulting far-field blooming in LPS-LDs that conventional wide-stripe LDs suffer from. Within the range $0 < n <$ N-1 lasing modes competition can lead to beam profile fluctuations at CW drive current changes, but the overall beam divergence is stabilized. Such lateral stability of a non-Gaussian laser beam profile can be interesting for numerous applications.

Acknowledgments

The work supported by the internal ITME project "Stabilization of emitted beam profile in junction plane of high-power laser diodes".

Conflict of interest

The authors declare that there is no conflict of interest in this paper.

References

1. Larsson A, Salzman J, Mittelstein M, et al. (1986) Lateral coherence properties of broad-area semiconductor quantum well lasers. *J Appl Phys* 60: 66–68.
2. Chow WW, Depatie D (1988) Filamentation in conventional double heterostructure and quantum well semiconductor lasers. *IEEE J Quantum Elect* 24: 1297–1301.
3. Chang-Haspain CJ, Kapon E, Colas E (1990) Spatial mode structure of index-guided broad-area quantum-well lasers. *IEEE J Quantum Elect* 26: 1713–1716.
4. Dente GG (2001) Low confinement factors for suppressed filaments in semiconductors lasers. *IEEE J Quantum Elect* 37: 1650–1653.
5. Asatsuma T, Takiguchi Y, Frederico S, et al. (2006) Successive phase change and stability of near-field patterns for broad-area laser diodes. *High-Power Diode Laser Technology and Applications IV* 6104: 61040C.
6. Tachikawa T, Takimoto S, Shogenji R, at al. (2010) Dynamics of broad-area semiconductor lasers with short optical feedback. *IEEE J Quantum Elect* 46: 140–149.
7. Wenzel H, Crump P, Ekhteraei H, et al. (2011) Theoretical and experimental analysis of the lateral modes of high-power broad-area lasers. *2011 Numerical Simulation of Optoelectronics Devices:* 143–144.
8. Crump P, Boldicke S, Schultz CM, et al. (2012) Experimental and theoretical analysis of the dominant lateral waveguiding mechanism in 975 nm high power broad area diode lasers. *Semicond Sci Tech* 27: 045001.
9. Piprek J (2013) Self-consistent far-field blooming analysis for high-power Fabry-Perot laser diodes. *Physics and Simulation of Optoelectronic Devices XXI* 8619: 861910.
10. Winterfeldt M, Crump P, Wenzel H, et al. (2014) Experimental investigation of factors limiting slow axis beam quality in 9xx nm high power broad area diode lasers. *J Appl Phys* 116: 063103.

11. Ripper JE, Paoli TL (1970) Optical coupling of adjacent stripe-geometry junction lasers. *Appl Phys Lett* 17: 371–373.
12. Scifres DR, Lindstrom C, Burnham RD, et al. (1983) Phase-locked (GaAl)As Laser diode emitting 2.6 W CW from a single mirror. *Electron Lett* 19: 169–171.
13. Marshall W, Katz J (1986) Direct analysis of gain-guided phase-locked semiconductor laser arrays. *IEEE J Quantum Elect* 22: 827–832.
14. Chaly VP, Karpov SY, Ter-Martirosyan AL, et al. (1996) Mechanisms of optical confinement in phase-locked laser arrays. *Semicond Sci Tech* 11: 372–379.
15. Maximov MV, Shernyakov YM, Novikov II, et al. (2008) High-power low-beam divergence edge-emitting semiconductor lasers with 1- and 20D photonic bandgap crystal waveguide. *IEEE J Sel Top Quant* 14: 1113–1122.
16. Sobczak G, Maląg A (2012) Optimization of phase-locked arrays geometry for high-brightness laser systems. *Opto-electron Rev* 20: 134–137.
17. Liu L, Zhang J, Wang Y, et al. (2012) 500-mW CW single-lobe emission from laterally coupled photonic crystal laser arrays. *IEEE Photonic Tech Lett* 24: 1667–1669.
18. Borruel L, Sujecki S, Rodriguez D, et al. (2003) Beam filamentation and maximum optical power in high brightness tapered lasers. *Physics and Simulation of Optoelectronic Devices XI* 4986: 423–431.
19. Wenzel H, Crump P, Fricke J, et al. (2013) Suppression of high-order lateral modes in broad-area diode lasers by resonant anti guiding. *IEEE J Quantum Elect* 49: 1102–1108.
20. Leidner JP, Marciante JR (2012) Beam quality improvement in broad-area semiconductor lasers via evanescent spatial filtering. *IEEE J Quantum Elect* 48: 1269–1274.
21. Qiao Z, Zhang S, Gao X, et al. (2010) Broad area semiconductor lasers with tailored gain. *Laser Physics and Laser Technologies (RCSLPLT) and 2010 Academic Symposium on Optoelectronics Technology (ASOT)*: 90–92.
22. Sun W, Pathak R, Campbell G, et al. (2013) Higher brightness laser diodes with smaller slow axis divergence. *High-Power Diode Laser Technology and Applications XI* 8605: 8605D.
23. Piprek J (2013) Inverse thermal lens effects on the far-field blooming of broad area laser diodes. *IEEE Photonic Tech Lett* 25: 958–960.
24. Takimoto S, Tachikawa T, Shogenji R, et al. (2009) Control of spatio-temporal dynamics of broad-area semiconductor lasers by strong optical injection. *IEEE Photonnic Tech Lett* 21: 1051–1053.
25. An H, Xiong Y, Jiang CL, et al. (2014) Methods for slow axis beam quality improvement of high power broad area diode lasers. *High-Power Diode Laser Technology and Applications XII* 8965: 89650U.
26. Yanson D, Levy M, Peleg O, et al. (2015) Low-NA fiber laser pumps powered by high-brightness single emitters. *High-Power Diode Laser Technology and Applications XIII* 9348: 934806.
27. Kanskar M, Bao L, Chen Z, et al. (2015) High brightness diodes & fiber-coupled modules. *High-Power Diode Laser Technology and Applications XIII* 9348: 934804.
28. Winterfeldt M, Crump P, Knigge S, et al. (2015) High beam quality in broad area lasers via suppression of lateral carrier accumulation. *IEEE Photonic Tech Lett* 27: 1809–1812.
29. Liu G, Li J, Fan L, et al. (2017) High power single lateral mode 1050 nm laser diode bar. *High-Power Diode Laser Technology XV* 10086: 10086Y.

30. Rieprich J, Winterfeldt M, Kerneke R, et al. (2018) Chip-carrier thermal barrier and its impact on lateral thermal lens profile and beam parameter product in high power broad area lasers. *J Appl Phys* 123: 125703.
31. Kanskar M, Bai C, Bao L, et al. (2019) High brightness diodes and 600W and 60% efficient fiber-coupled packages enabled by reduced-mode (REM) diodes. *High-Power Diode Laser Technology XVII* 10900: 109000H.
32. Yang JT, Kim Y, Lee JB, et al. (2019) Dependence of high-power laser diode performance on emitter width. *High-Power Diode Laser Technology XVII* 10900: 109000N.
33. Sobczak G, Dąbrowska E, Teodorczyk M, et al. (2014) Improvement of the lateral mode stability in high-power laser diodes by multi-stripe-gain distribution. *IEEE J Quantum Elect* 50: 890–897.
34. Wang T, Tong C, Wang L, et al. (2016) Injection-insensitive lateral divergence in broad-area diode lasers achieved by spatial current modulation. *Appl Phys Express* 9: 112102.
35. Maląg A, Dąbrowska E, Teodorczyk M, et al. (2012) Asymmetric heterostructure with reduced distance from active region to heatsink for 810-nm range high-power laser diodes. *IEEE J Quantum Elect* 48: 465–471.
36. Tachikawa T, Takimoto S, Shogenji R, et al. (2010) Dynamics of broad-area semiconductor lasers with short optical feedback. *IEEE J Quantum Elect* 46: 140–148.
37. Sobczak G (2015) Improvement of the quality of the beam emitted by edge-emitting laser diodes through the lateral periodicity of heterostructure waveguide. Ph.D. Thesis.
38. Kozłowska A, Maląg A, Dąbrowska E, et al. (2012) Thermal properties of high-power diode lasers investigated by means of high resolution thermography. *Mat Sci Eng B* 177: 1268–1272.
39. Talghader J, Smith JS (1995) Thermal-dependence of the refractive-index of GaAs and AlAs measured using semiconductor multilayer optical cavities. *Appl Phys Lett* 66: 335–337.
40. Maląg A, Sobczak G, Dąbrowska E (2018) Emitted beam stabilization in junction plane by lateral periodic structure in laser diodes emitting at 980 nm. *Laser Technology 2018: Progress and Applications of Lasers* 10974: 1097404.
41. Martin D, Della Casa P, Adam T, et al. (2019) Current spreading suppression by O- and Si-implantation in high power broad area diode lasers. *High-Power Diode Laser Technology XVII* 10900: 109000M.

AIMS Press

© 2019 the Author(s), licensee AIMS Press. This is an open access article distributed under the terms of the Creative Commons Attribution License (http://creativecommons.org/licenses/by/4.0)